Available online at www.sciencedirect.com
SCIENCE DIRECT
Atmospheric Environment 40 (2006) 1909–1921
ATMOSPHERIC ENVIRONMENT
www.elsevier.com/locate/atmosenv

Seasonal and interannual variability in absorbing aerosols over India derived from TOMS: Relationship to regional meteorology and emissions

Gazala Habib[a], Chandra Venkataraman[a,*], Isabelle Chiapello[b], S. Ramachandran[c], Olivier Boucher[b,1], M. Shekar Reddy[b,2]

[a]*Department of Chemical Engineering, Indian Institute of Technology Bombay, Powai, Mumbai-400 076, India*
[b]*Laboratoire d'Optique Atmosphérique, CNRS UFR de Physique, Bat P5, Universite de Lille, 59655Villeneuve d'Ascq Cedex, France*
[c]*Space and Atmospheric Sciences Division, Physical Research Laboratory, Navrangpura, Ahmedabad 380 009, India*

Received 25 April 2005; received in revised form 31 July 2005; accepted 31 July 2005

Abstract

The objective of this study is an analysis of the spatial, seasonal and interannual variability of regional-scale aerosol load over India, detected by TOMS during 1981–2000, with an evaluation of potential contributing factors, including estimated anthropogenic aerosol emission trends and regional meteorology (rainfall and circulation patterns). Spatial distributions in TOMS Ai were related to the emission densities of anthropogenic absorbing aerosols in April–May, but varied seasonally and were modified significantly by higher atmospheric dispersion in January–March and rainfall in June–September, both of which lead to low TOMS Ai, even in regions of high aerosol emissions. Dust emissions explain the high TOMS Ai over northwest region during April–May and June–September when rainfall is scanty and significant air-mass decent occurs in this region. The magnitude of TOMS Ai correlated with the anthropogenic absorbing aerosol (black carbon and inorganic matter) emission flux in five selected regions, dominated by biomass/biofuel burning and fossil fuel combustion, but not in a region with significant mineral dust emissions. The seasonal cycle in TOMS Ai was related to the seasonal variability in dust, biomass burning emissions and rainfall. Interannual variability in TOMS Ai was linked to that in forest burning emissions in the northeast, as evidenced by a correlation with ATSR fire-counts, both significantly enhanced in 1999. Trends in anthropogenic emissions during 1981–2000 potentially contribute to increases in the aerosol load detected by TOMS. This would need further investigation using analysis incorporating both trends in anthropogenic emissions and the interannual variability in natural sources of aerosols.

Keywords: Aerosols; Long-term trends; Satellite remote sensing; Emission inventory; Rainfall; Regional circulation

1. Introduction

Large uncertainties are associated with the prediction of climate effects of aerosols (Boucher and Haywood, 2001; Anderson et al., 2003), arising in part from their high temporal and spatial

*Corresponding author. Tel.: +22 25764239; fax: +22 25723480.
E-mail addresses: chandra@che.iitb.ac.in, chandra@iitb.ac.in (C. Venkataraman).
[1]Now at the Met Office, Exeter, UK.
[2]Now at NOAA/Geophysical Fluid Dynamics Laboratory, Princeton, USA.

1352-2310/$ - see front matter © 2005 Published by Elsevier Ltd.
doi:10.1016/j.atmosenv.2005.07.077

variability. Variability in aerosol loading over tropical India has been recorded through observational networks. For example, long-term measurements, made using a network of multi-wavelength radiometers, showed increases of 2–9% yr^{-1} in columnar aerosol optical depth at 400 nm, at locations like Trivandrum (8.5°N, 76.9°E; coastal), Vishakapatnam (17.7°N, 83.2°E; industrialized) and Mysore (12.3°N, 76.5°E; continental) during 1986–1998 (Moorthy et al., 1993; Moorthy et al., 2001). Upper tropospheric aerosol extinction coefficients, derived from balloon-borne sun scanning/tracking photometers at Hyderabad (17.5°N, 78.6°E) (Ramachandran and Jayaraman, 2003), increased by about $11 \pm 1\%\ yr^{-1}$ during 1985–2001. Extensive aerosol optical and chemical measurements during the Indian Ocean Experiment (INDOEX) (Ramanathan et al., 2001) showed significant concentrations of absorbing aerosols and associated optical depth during the NE monsoon (January–March), along with a large interannual variability in these parameters (Moorthy et al., 2001; Li and Ramanathan, 2002; Ramachandran, 2004). Analysis of optical depth measurements at Kaashidhoo (Maldives, 4.9°N, 73.5°E), from AERONET, and Minicoy (8.3°N, 73.1°E), from radiometer measurements, in the near-IR at 1020 nm, indicated that dust, transported from NW India, and the Arabian and Saharan regions, dominate the aerosol optical depth during April–May (Satheesh and Srinivasan, 2002).

Here it is our interest to undertake an analysis of the spatial, seasonal and interannual variability of aerosol load over India on a regional-scale with an analysis of potential contributing factors. Satellite remote sensing has been successfully applied in deducing the origin, temporal and spatial distribution of absorbing aerosols (Herman et al., 1997; Torres et al., 1998; Chiapello et al., 1999), and in constraining biomass-burning emissions (Duncan et al., 2003). The Advanced Very High-Resolution Radiometer (AVHRR) aerosol data set provides information on aerosol optical depth limited, however, to water surfaces (Husar et al., 1997). The positively constrained spectral contrast in the ultra-violet (UV) range derived from Total Ozone Mapping Spectrometer (TOMS), termed TOMS aerosol index (TOMS Ai), has been successfully used to detect absorbing aerosols (i.e. desert mineral dust and smoke aerosol from biomass burning) in the UV range, both on land and ocean (Hsu et al., 1996; Herman et al., 1997; Chiapello et al., 1999; Duncan et al., 2003).

Correlations were found between TOMS Ai and sun photometer aerosol optical depth measurement for regions like Saharan desert, Atlantic Ocean, South America (Torres et al., 1998; Hsu et al., 1999) and with aerosol mass concentrations, for example, those measured over the North Atlantic ocean (Chiapello et al., 1999).

The long-term TOMS data set from 1979 to present recorded from a succession of satellite platforms (Nimbus 7: 1979–1993; Meteor 3: 1991–1994; ADEOS-1: 1996–1997; Earth Probe: 1996-present) provides a unique opportunity for an analysis of the long-term evolution of aerosol loading over the Indian subcontinent. Therefore, the objectives of this study include (a) an analysis of the spatial and seasonal variability of absorbing aerosol load over India using TOMS Ai, and (b) a study of the interannual variability of absorbing aerosol loading during 1981–2000, over selected Indian regions characterized by different aerosol sources, and its relationship to regional meteorology and anthropogenic aerosol emissions.

2. Database and methodology

2.1. TOMS aerosol product

TOMS has been designed for the estimation of the total-column ozone from the measured amount of backscattered UV radiance in six 1-nm wide wavelength bands (313, 318, 331, 340, 360 and 380 nm) (Herman et al., 1997). At the three longest wavelength bands (340, 360 and 380 nm) gaseous absorption is weak, and the net aerosol effects on backscattered radiation is primarily governed by competing radiative transfer processes including Rayleigh and Mie multiple scattering, aerosol absorption of both Rayleigh and Mie scattered radiation as well as scattering and absorption of radiation reflected by underlying surface (Torres et al., 1998). The algorithm for TOMS detection of aerosol and clouds from the backscattered UV radiance measurement is based on the residue theory described in Herman et al. (1997) and Torres et al. (1998). The residue method is based on the principle that for a fixed 380 nm radiance the I_{340}/I_{380} spectral contrast is largest for non-absorbing aerosol and clouds and decreases with increasing absorption. UV absorbing aerosols (dust, smoke, soot) produce smaller contrast than predicted by

pure Rayleigh scattering atmospheric model, consequently they yield positive residues. In contrast the non-absorbing aerosols (sulfate and sea-salt particles) produce greater contrast and negative residues. These positive or negative residues are termed as Ai.

Absorption by UV absorbing aerosol is strongly altitude dependent and increases with increase in altitude because these aerosols strongly absorb the molecular radiation coming from below, i.e. higher the aerosol altitude greater the fraction of affected molecular radiation. This can lead to underestimation of aerosols confined at low level (Torres et al., 1998). The other sources of uncertainties are the particles UV refractive index and presence of cloud. Thus, as mentioned by Torres et al. (1998), weakly absorbing aerosols at low altitude yield negative residues and cannot be distinguished from non-absorbing aerosols. Subpixel cloud contamination can underestimate the aerosols even though clouds themselves are much brighter than the aerosols (Torres et al., 1998).

Here, we consider only the positive values of TOMS Ai (hereafter TOMS Ai in this paper), corresponding to absorbing aerosol loading. The association of TOMS Ai with specific types of absorbing aerosols is largely based on the comparison of temporal and spatial variability of TOMS aerosol index (Ai) with known source of these aerosols (Herman et al., 1997). Four different TOMS instruments flew in space since November 1978 (Herman et al., 1997). Here we use TOMS data from Nimbus 7 for the years 1981–1992 and from Earth-Probe for the years 1997–2000. Since the latest instrument does not contain wavelengths at 340 and 380 nm, the aerosol index is calculated using the 330–360 nm range, the Ai being nearly a linear function of wavelength over the 330 and 360 nm. It is recommended that TOMS Ai from Nimbus 7 (1981–1992) be scaled by a factor of 0.75 for comparison with those from Earth Probe (1997–2000) (Hsu et al., 1999) and this is followed in the present work. However, as explained in a following section, our analysis shows that the data sets of TOMS Ai for the two periods, 1981–1992 and 1997–2000, were statistically from different populations, thus requiring separate analysis.

2.2. Estimating absorbing aerosol emissions over India

To study the seasonal and interannual variability in absorbing aerosol load, in relation to emissions and regional meteorology, we chose six regions of India, dominated by emissions from different sources, i.e. biomass burning, fossil fuel combustion or desert dust.

2.2.1. Methodology for estimating aerosol emission trends and distributions

We classify anthropogenic absorbing aerosols to include black carbon (BC, predominantly from biomass burning in this region) and inorganic oxidized matter (IOM, mostly fly ash from coal fired power plants, followed by mineral matter from open burning of crop waste and forests) (Reddy and Venkataraman, 2002a, b). Soluble inorganic constituents like sulfate were not included in IOM. Detailed biofuel used for cooking (Habib et al., 2004) are projected using national population for the period 1981–2000 from Government of India census data (http://www.censusindia.org.in). Crop waste generation trends are estimated from annual crop production for 1981–2000 (Chanda et al., 2001) and related residue-to-product ratios (Shrivastava, 2003). Crop waste burnt in field is derived from the crop waste generated and the national average fraction burnt (i.e. crop waste burnt as a percentage of crop waste generated) 12% (Reddy et al., 2002). Emission factors of BC and IOM for biofuel combustion (Venkataraman et al., 2005; Reddy and Venkataraman, 2002b), crop waste open burning (Reddy et al., 2002) and forest fires (Reddy and Venkataraman, 2002b) are used to estimate emission trends.

Fossil fuel use trends have been taken from Center for Monitoring Indian Economy (Centre for Monitoring Indian Economy (CMIE), 2001) for coal, low- and high-speed diesel, petrol (motor gasoline), fuel (furnace) oil, and kerosene (detailed in Ramachandran and Jayaraman, 2003). Differences in emissions between this work and the detailed emission inventory for 1996 with emission factors based on technology and fuel consumption (Reddy and Venkataraman, 2002a), arose from the use of sector average emission factors by Ramachandran and Jayaraman (2003). Scaling factors of 2.0 and 0.65 were applied, respectively, to BC and IOM, to make the emissions trends of Ramachandran and Jayaraman (2003), for fossil fuels, consistent with the detailed inventory.

Climatological monthly mean BC emissions from forest fires have been derived by combining the source term with fire counts from ATSR (Along-Track Scanning Radiometer aboard satellite ERS-2)

(Reddy and Boucher, 2004) averaged for the period 1996–2000, at a resolution of $1^\circ \times 1^\circ$ over the Indian region. Forest burning is assumed to have negligible long-term variability and the climatological mean emissions of BC and IOM derived thus was added as a constant component to the national emissions during 1981–2000. However, for an analysis of interannual variability of TOMS Ai in northeast India, variation in ATSR fire counts has been derived as monthly mean during 1997–2000 in this region. In spite of potential biases in the ATSR fire-counts, caused by pixel-size, night-time and clear-sky sampling, this approach permits better representation of seasonal variations in forest burning on regional scales (Duncan et al., 2003; Generoso et al., 2003; Reddy and Boucher, 2004). Spatial distributions of absorbing aerosol emissions are developed for the year 2000, using appropriate proxies to distribute state-level emissions to districts as done previously (Reddy and Venkataraman, 2002a, b) and gridded at a $0.25^\circ \times 0.25^\circ$ resolution.

2.2.2. Sources and chemical composition of regional aerosol emission fluxes

We use the ratio of the gridded aerosol emissions for the year 2000, from fossil fuel to biomass burning, in order to identify the dominant sources of aerosols in each Indian region. Fig. 1 shows low overall emission ratio from fossil fuels (light gray squares), suggesting that biomass burning sources (biofuel, crop waste open burning and forest fires) dominate most grids. However, sources like power plants, cement plants, refineries and iron and steel plants, dominate the emissions in several individual grids (dark gray and black squares in Fig. 1). Northeast India (R1) and Bengal/Orissa (R2), chosen to represent biomass burning regions, are characterized by a large frequency of ATSR fire-count signals as shown in previous studies (Duncan et al., 2003; Reddy and Boucher, 2004). Air-masses advected over the Indo-Gangetic plain (R3), south (R4) and west (R5), chosen as the fossil fuel dominated regions in this work, have been shown to contain high concentrations of anthropogenic aerosol constituents by recent field measurements (Novakov et al., 2000; Ramanathan et al., 2001; Gabriel et al., 2002; Mayol-Bracero et al., 2002). A desert dust dominated region (R6) has been defined in the northwest of India, based on the dust emission inventory of Tegen and Fung (1995). Fig. 2 shows that the emission fluxes are the largest in the Indo-Gangetic plain (R3) followed by the other fossil fuel dominated regions (R4 and R5). The biomass burning regions (R1 and R2) exhibit lower emission fluxes, from their lower population density and industrialization, related to the predominantly forest land cover. The fossil fuel regions show significantly greater mixed sources (28–38% biomass contribution) than biomass burning regions (15–18% fossil fuel contribution). The desert dust dominated region, is characterized by a low anthropogenic emission flux, dominated by biomass burning. A large fraction of the anthropogenic $PM_{2.5}$ (or fine particle) emissions are contributed by absorbing anthropogenic aerosols (9–18% BC and 35–69% IOM) in the selected regions. Particulate matter emissions are dominated by carbonaceous aerosols in the biomass burning regions (R1 and R2) and by IOM in the fossil fuel regions (R3–R5).

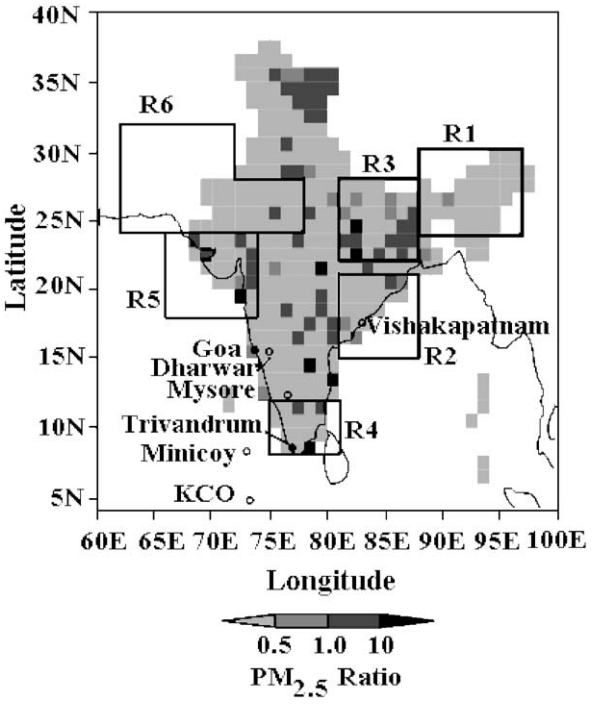

Fig. 1. Ratio of $PM_{2.5}$ emission fluxes ($kg\,km^{-2}\,yr^{-1}$) from fossil fuel to biomass burning. Regions selected for analysis are R1 (24–30°N; 88–97°E), R2 (15–21°N; 81–88°E) dominated by biomass burning, R3 (22–28°N; 81–88°E), R4 (8–12°N; 75–81°E), and R5 (18–24°N; 66–74°E) dominated by fossil fuel and R6 (28–32°N, 68–72°E; 24–28°N, 62–78°E) desert dust dominated. The ground stations Trivandrum (8.5°N, 76.9°E; coastal), Vishakapatnam (17.7°N, 83.2°E; industrialized) and Mysore (12.3°N, 76.5°E; continental), Minicoy (8.3°N, 73.1°E) have been chosen for comparison TOMS Ai with measured AOD. The ground stations chosen for analysis of pollution events at daily time scale during INDOEX are Goa (15.5°N, 73.8°E)/ Dharwar (15.4°N, 74.9°E) and Kaashidhoo (4.9°N, 73.5°E).

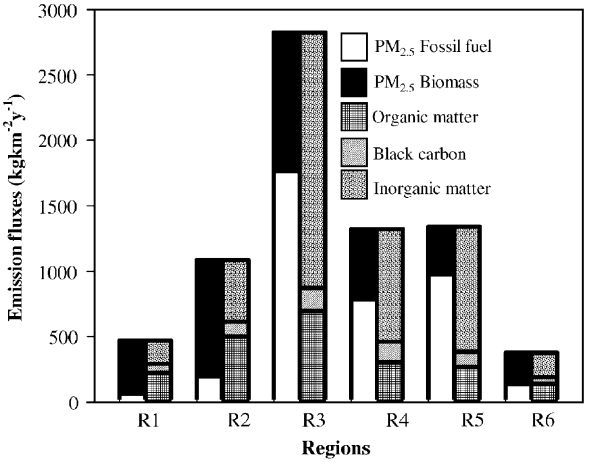

Fig. 2. Emission fluxes (kg km^{-2} yr^{-1}) of $PM_{2.5}$ and BC, OM and IOM in regions dominated by biomass burning (R1 and R2), fossil fuel combustion (R3, R4, and R5) and desert dust (R6) emissions.

BC is emitted primarily from biomass burning in all regions. IOM matter is largely emitted from coal-fired utilities in the fossil fuel regions, while in the biomass-dominated regions, it is emitted primarily from biofuel combustion in the northeast (R1), but from forest burning in the east (R2). Organic matter (OM) and BC emissions in India are strongly correlated, particularly from biomass burning and brick kiln dominated regions (Reddy and Venkataraman, 2002a, b) and may have an absorbing character (Reddy and Boucher, 2004; Reddy et al., 2004). This implies that the aerosols are likely to be chemically mixed.

2.3. Rainfall data

We analyze regional rainfall data to examine the potential effect of rainfall on spatial and temporal variability of aerosol loading detected by TOMS. Rainfall in India is governed by the southwest monsoon (July–September), or Indian summer monsoon, which contributes to 77% of the annual national rainfall. Gadgil et al. (2002) have analyzed the SW monsoon using 130 years (1871–2001) of rainfall data and reported 70% of the years with normal rainfall, about 15% with drought and 15% with excess rainfall, and a strong natural variability. To analyze the effects of this variability on aerosol loading, rainfall data are obtained for 29 subdivisions of India (http://www.tropmet.res.in) for the 20-year period (1981–2000). These data are compiled from a network of 306 rain gauge stations in the 29 meteorological subdivisions, which cover 90% of the total area of the country. In addition, the 100-year average (1901–2000) of monthly mean rainfall is calculated in the selected regions. Monthly mean subdivisional rainfall is aggregated to derive the monthly mean rainfall and monsoon index (June–September rainfall, corresponding to the southwest monsoon) in selected regions.

2.4. NCEP reanalysis data

To evaluate the potential effect of regional circulation changes on the aerosol load detected by TOMS, we analyze vertical velocity (Pa s^{-1}) to identify regions with significant air-mass ascent, leading potentially to aerosol dispersion, or descent, leading to confinement of emissions, and possible higher aerosol loading. NCEP reanalysis data are downloaded from the web site of the NOAA-CIRES Climate Diagnostics Center, Boulder, CO, at http://www.cdc.noaa.gov. An examination of the monthly mean vertical velocity at 500 and 850 hPa showed a significant seasonal and interannual shift in the regional circulation pattern. While the direction of vertical air-mass velocity at 850 and 500 hPa remained unchanged in most months, the spatial contrast was more clearly seen in the data at 500 hPa. Therefore, monthly mean vertical velocities at 500 hPa are used as an index of the dispersive potential of the atmosphere. The long-term average (1958–present) of monthly mean vertical velocity over India typically ranged 0.02–0.06 Pa s^{-1}, with an interannual standard deviation below 0.02 Pa s^{-1}.

3. Results and discussion

3.1. Seasonal and spatial variability in TOMS Ai and relation to regional meteorology

3.1.1. Spatial distributions in different seasons

Fig. 3 shows the seasonal variability of TOMS Ai spatial distributions for the year 2000, for three periods of the year corresponding, respectively to the NE monsoon (January–March), the dry season (April–May) and the SW monsoon (June–September). In October–December (not shown), meteorological conditions are similar to January–March, however with NE monsoon rainfall in south India. The spatial variability of TOMS Ai in each season is analyzed using absorbing aerosol emissions and potential aerosol sinks, like rainfall and atmospheric dispersion. Distributions of seasonal

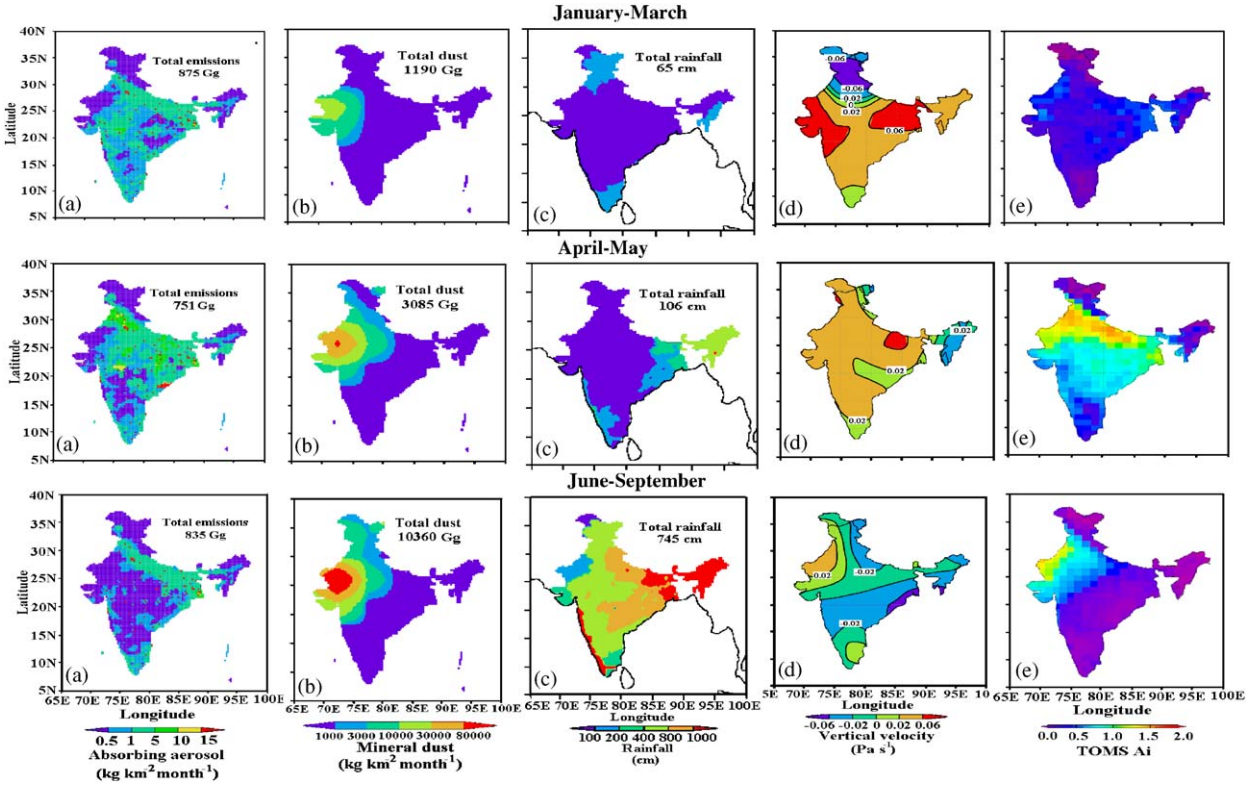

Fig. 3. Seasonal variability in distributions of (a) emissions of BC and IOM aerosols, (b) emissions dust, (c) rainfall, (d) mean vertical velocity at 500 hPa, and (e) TOMS Ai over India, for the year 2000 during NE monsoon (top panel), (b) dry season (middle panel), (c) SW monsoon (bottom panel).

average rainfall over India are based on the data of year 2000. Monthly mean vertical air-mass velocities at 500 hPa from NCEP reanalysis data are used as an index of atmospheric dispersion, to identify regions with significant air-mass ascent, leading potentially to aerosol dispersion and low atmospheric loading, or descent, leading to confinement of aerosol emissions and possible higher loading.

During January–March (Fig. 3, top panel), distributions of emissions show large fluxes of anthropogenic absorbing aerosol emissions in Indo-Gangetic plain, Bengal (east), east coast plains and south India, with an additional peak in the west (Fig. 3a). In addition to this the dust emissions were seen over the northwest (Thar desert) and some parts of the west (Fig. 3b). However, the TOMS signal is low throughout and does not show a pattern similar to the emissions distributions (Fig. 3e). This difference cannot be explained by rainfall, which in this season is scanty over most of India (Fig. 3c). The circulation pattern, in terms of the estimated NCEP vertical velocity at 500 hPa, averaged for January–March 2000, shows significant air-mass ascent (purple and green) over the north Indo-Gangetic plain and descent (red) over central and eastern part of Indo-Gangetic plain of India (Fig. 3d). The air-mass ascent over the Indo-Gangetic plain, could potentially result in significant dispersion of emissions from this region leading to the low absorbing aerosol loading detected by TOMS.

In the dry season (Apr–May) (Fig. 3, middle panel), aerosol emissions from the Indo-Gangetic plain are accompanied by emissions from central India from forest fires and open burning of crop-waste (Fig. 3a). In addition, mineral dust emissions arise from the northwest and west desert regions (Fig. 3b) and long-range transport from Africa and west-Asia (Satheesh and Srinivasan, 2002). The TOMS signal shows corresponding high Ai over the Indo-Gangetic plain and northwest India. In this season once again there is insignificant rainfall over the subcontinent (Fig. 3c) and insignificant

aerosol removal through scavenging. The regional circulation pattern shows significant air-mass descent (red) over the Indo-Gangetic plain and northwest (Fig. 3d). This can potentially limit dispersion and lead to high loading of aerosols over the Indo-Gangetic plain, detected in the TOMS signal (Fig. 3e).

During the SW monsoon (June–September) (Fig. 3, bottom panel), aerosol emissions continue to be high in the Indo-Gangetic plain and parts of South, and West India (Fig. 3a). However, TOMS Ai shows a low signal over the entire subcontinent, except for a high in the northwest (Fig. 3e). The dust emissions continued to be high in northwest and the western Indo-Gangetic plain (Fig. 3b). In this season, most parts of India receive southwest monsoon rainfall, leading to the low TOMS signal (Fig. 3c). Aerosol detection by TOMS can also be obscured by the presence of cloud during monsoon period, resulting in underestimation of aerosol load in cloudy regions. However, the high TOMS Ai in the northwest is coincident with the desert region, where dust emission continues during June–September and about three times higher than the dry season (Fig. 3b, middle and bottom panel). In addition to the low-to-medium rainfall in the northwest during this season, the high air mass descents (increased subsidence) (Fig. 3d) in the troposphere will lead to low-level confinement of aerosols.

In October–December (not shown), the emissions and meteorological conditions are similar to January–March, and south India receives rainfall from the NE monsoon. TOMS Ai is low throughout the subcontinent during this season as in January–March. The study by Di Girolamo et al. (2004) has shown significantly high aerosol load over Indo-Gangetic plain during December–February averaged over the year 2001–2004 using the aerosol optical depth from Multi-angle Imaging Spectro-Radiometer (MISR). This discrepancy in TOMS aerosol retrieval could result from factors including low aerosol altitude and mixture of absorbing and non-absorbing aerosols (Torres et al., 1998).

Overall, beside the limitations including cloud cover, aerosol height and mixing of absorbing and non-absorbing aerosol TOMS Ai have shown some interesting relationship with anthropogenic and dust emissions over Indian region. Especially, the spatial distributions of absorbing aerosols detected by TOMS, exhibit a good relation to anthropogenic and dust emissions distributions on a subcontinental scale during dry season (April–May), when rainfall and dispersion are insignificant. However, atmospheric dispersion on a regional scale (as in Jan–March over North India) and rainfall (as in June–September) reduce aerosol loads and modify their spatial distributions in relation to their anthropogenic emissions over most of the Indian subcontinent. The northwest desert region seems to be an exception with large dust emissions accompanied by scanty rainfall and significant air mass decent in June–September, resulting in high dust loads corresponding to highs in TOMS Ai.

3.1.2. *Monthly variability in selected regions*

Monthly mean TOMS Ai are extracted and spatially averaged over the six selected regions shown in Fig. 1, dominated by different aerosol sources, and described in Section 2.3. As explained earlier, TOMS Ai from Nimbus 7 (1981–1992) were scaled by the recommended factor of 0.75 for direct comparison with those derived from TOMS/Earth-Probe (1997–2000) (Hsu et al., 1999). In spite of this, in all selected regions, the data sets from Nimbus 7 and Earth Probe, when tested using a *t*-test, at 95% statistical significance, were seen to come from different populations, not making it possible to pool the datasets in our analysis. Therefore, in all the following sections, the data sets from 1981–1992 to 1997–2000 are treated separately.

Fig. 4a–f shows the monthly mean TOMS Ai spatially averaged over each region for the period 1981–1992, with one standard deviation shown by error bars. Also shown in each region, is the monthly mean rainfall, averaged over the same period, using the rainfall data described in Section 2.3, from the meteorological subdivisions corresponding to each region. The northeast and east (R1 and R2) are dominated by biomass burning emissions (Fig. 2), of which biofuel combustion emissions are invariant with season, and open burning emissions are predominant in March–May. The peak TOMS Ai in the northeast is in April, when onset of rainfall reduces the aerosol load (Fig. 4a). In the east (R2), the peak TOMS Ai is in May, from the later onset of rainfall in June, after which once again, the increasing rainfall decreases aerosol load (Fig. 4b). The Indo-Gangetic plain (R3) has the largest absorbing aerosol fluxes among the six regions, with about 60% from fossil fuel combustion, typically invariant with season, and 40% from biomass burning (Fig. 2), thus with an expected

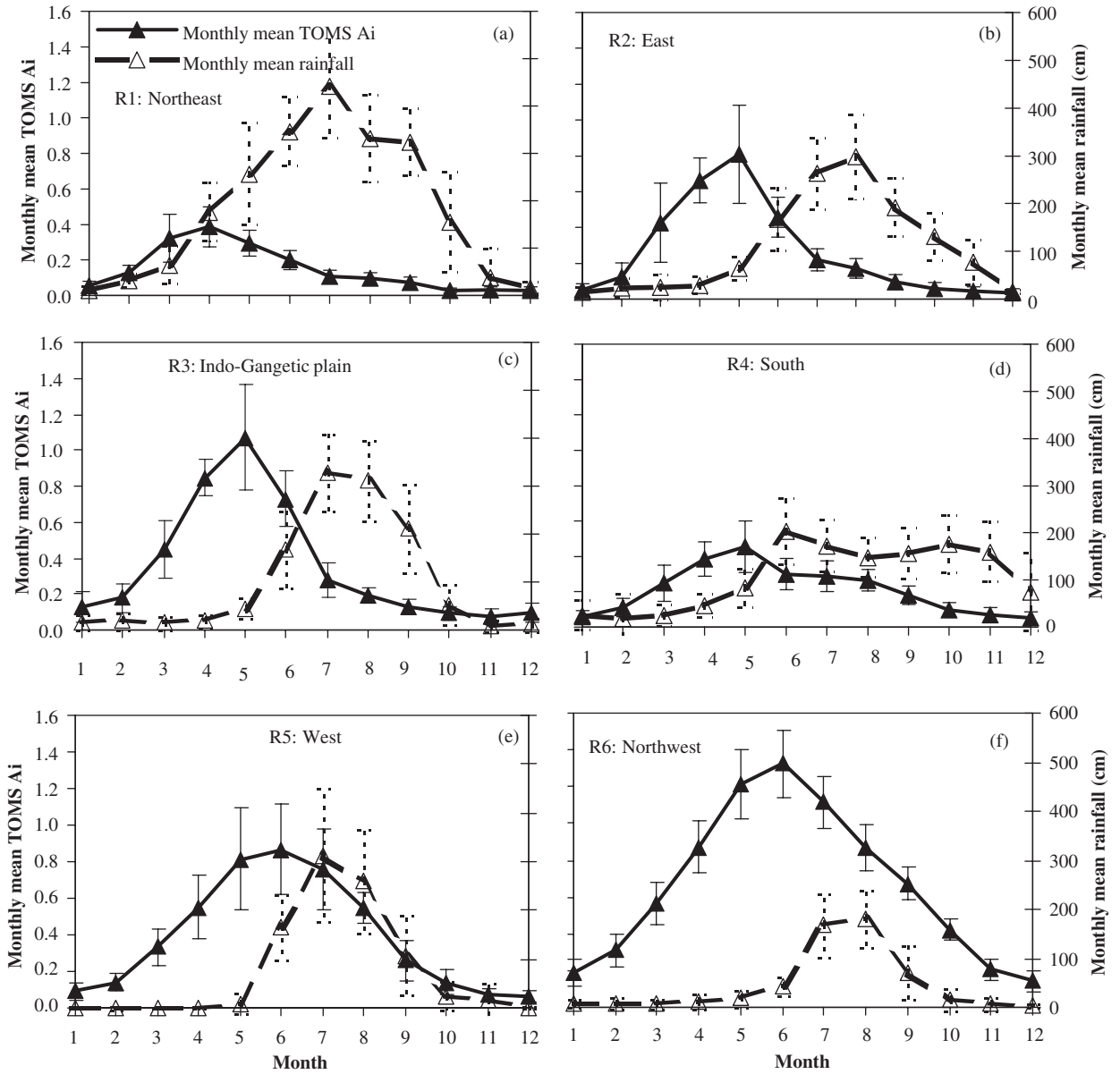

Fig. 4. Seasonal cycle in the TOMS Ai (solid lines with filled triangles) and in rainfall (dotted lines with open triangles) in six selected regions (R1–R6).

lower seasonal variation in emissions than east or northeast. However, the similar monthly rainfall distribution in the Indo-Gangetic plain, to that in the east, results in a seasonal cycle in TOMS Ai very similar to that in the east (Fig. 4c). The south (R4) has mixed emissions with almost equal fluxes from biomass and fossil fuel burning (Fig. 2). The distinct features of this region include a harvest season in Janury–February, leading to potential open burning emissions in these months, and the influence of both southwest and northeast monsoon rainfall. The peak rainfall in this region is 100–200 cm month^{-1}, lower than in R1–R3, but persisting from June–November. The peak TOMS Ai has a lower value than in R2 and R3, from the lower emissions flux in this region. It occurs in May, but does not fall off sharply as the rainfall amounts are lower than in the other regions. The west and northwest have lower anthropogenic aerosol fluxes (Fig. 2), but experience high dust load from the Thar desert, along with

more scanty rainfall than the other regions. High dust activity typically occurs in May–June. The seasonal cycle in TOMS Ai thus shows enhanced peak values in June, especially in the northwest, which is affected more by desert dust (Fig. 4e, f). The onset of rainfall in both regions is from July leading to a steady reduction in TOMS Ai. The combination of high dust load and low rainfall induces the largest values of TOMS Ai in these two regions. Therefore, the magnitude of TOMS Ai bore a relation to anthropogenic aerosol emission strength in all regions except those with a strong desert dust loading. The seasonal cycle in TOMS Ai was related primarily to the seasonal variability in

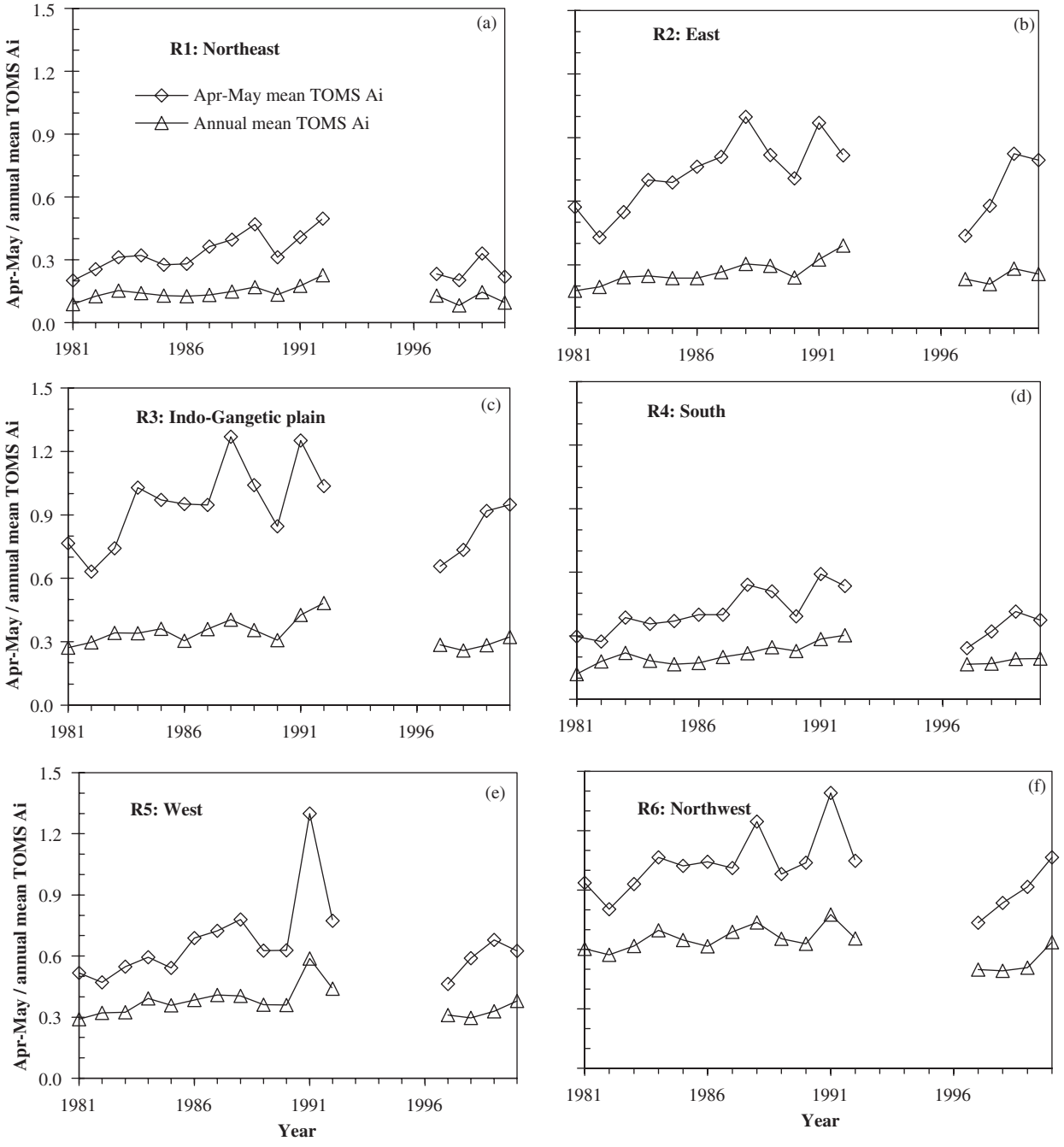

Fig. 5. Long-term variability in April–May and annual mean TOMS Ai in selected regions.

dust or open burning emissions and a large influence of rainfall in reducing the aerosol load.

3.2. Interannual variability in TOMS Ai

In the following discussion we analyze the year-to-year variability of the April–May mean TOMS Ai, which is always higher than the annual mean (Fig. 5) TOMS Ai and governs the annual mean in each region. Using the 1981–1992 data, the largest TOMS Ai is observed in the desert dust dominated region (R6, 1.00 ± 0.16), which result both from local dust emissions and potentially from long-range transport from the Arabian and Saharan desert regions, known to be active during April–May (Satheesh and Srinivasan, 2002). Moreover, TOMS Ai is more sensitive to dust aerosols and to aerosols at higher altitudes (Herman et al., 1997; Torres et al., 1998) potentially contributing to the high TOMS Ai recorded in this region. Among regions dominated by anthropogenic emissions, TOMS Ai follows trends in the magnitude of absorbing aerosol emission flux (Fig. 2), with highest TOMS Ai in the Indo-Gangetic plain (R3, 0.92 ± 0.19) followed by east and west (R2, 0.72 ± 0.17; R5, 0.66 ± 0.20), and significantly lower in the south and northeast (R4, 0.40 ± 0.10; R1, 0.32 ± 0.09).

3.2.1. Influence of emissions

Fig. 5 shows that during the period 1997–2000 the interannual variability of TOMS Ai in the northeast region R1, is characterized by exceptionally high TOMS Ai during 1999, about 1.5 times larger than in the other adjacent years. This region is known to be affected by forest biomass burning, with ATSR fires in 1999 seen to feature an intense area of burning along the foothills of the Himalaya in the Indo-Gangetic plain (Duncan et al., 2003, Reddy and Boucher, 2004). Variability in forest burning emissions is thus examined as a potentially dominant contributor to TOMS Ai in the northeast region. Monthly mean ATSR fire counts are derived for 1997–2000 in this region (Fig. 6) and ranged from 5 to 30 during March–May in 1997, 1998, and 2000 but recorded an exceptional peak of 329 during March 1999 (24 in April and 3 in May 1999). It should be noted that from July to December, ATSR detected no fires in this region, in contrast to the low, but still positive values of TOMS Ai during these months. This discrepancy may arise from differences in the overlap of fire duration and the sampling times of the ATSR sensor or potential biases from pixel size and clear-sky sampling (Arino et al., 2001). A comparison of ATSR with MODIS data (not available for the period of this study) shows that MODIS detected more fires during September–October 2001, than ATSR (results not shown). We broadly conclude that the co-variation of TOMS Ai with ATSR fires observed here, points to the role of BC emissions from forest fires in enhancing TOMS Ai in northeast India in 1999.

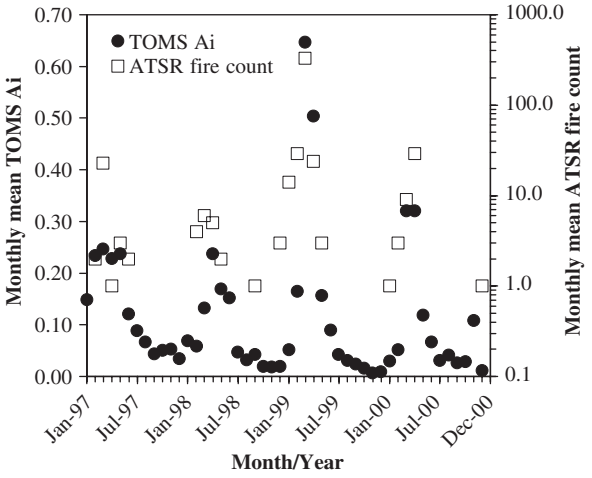

Fig. 6. Monthly mean of TOMS Ai and ATSR fire counts (excluding zero values) in the northeast region R1 dominated by open biomass burning from 1997 to 2000.

As meteorological parameters allow only to partially explain the interannual variability of TOMS Ai, we examine the influence of the variability of absorbing aerosol emissions, projected during 1981–2000, as described in Section 2.3. These projections (Fig. 7) show an increase in average emissions of BC from 235 in 1981 to 390 Gg in 2000 (i.e. a factor 1.6) and of IOM from 1190 in 1981 to 2520 Gg in 2000 (i.e. a factor 2.1). The increase in emissions from biomass burning of about 2% yr^{-1} is reflected by the growth rate in user population of biofuels (i.e. the rural population) and the increase in crop waste burnt as a function of growth in crop production during this period. Forest emissions were assumed invariant at the mean value estimated for 1996–2000. The increase in emissions from fossil fuel burning of about 9% yr^{-1} reflects an increase in industrial fossil fuel use, with BC being governed by diesel transport and IOM by coal use in electric power generation. These national average emissions are distributed to the six regions, based on the

regional distribution of emissions for the year 2000. While this approach assumes an invariant spatial distribution of emissions during the 20-year period, we believe it offers a reasonable first approximation of the decadal growth in regional emissions.

To arrive at the dependence of the year-to-year TOMS Ai on annual mean emissions, circulation effects and rainfall, a dataset is developed for each region of annual emissions, as described above, of NCEP vertical velocity at 500 hPa for April–May and of annual rainfall of the previous year, for the years 1981–1992. Interannual variability in TOMS Ai is examined simultaneously in relation to that in anthropogenic aerosol emissions, vertical velocity and rainfall from the year ($n-1$), using a multiple regression (Table 1). An important aspect missing from this analysis is an explicit treatment of the influence mineral dust emissions on TOMS Ai in the west and northwest, and of long-range transported dust on TOMS Ai in other regions. The interannual variability in TOMS Ai in all regions is explained largely (37–70%) by trends in anthropogenic aerosol emissions. Atmospheric circulation, in terms of vertical velocity, is not useful in explaining year-to-year variability in TOMS Ai. Rainfall from the ($n-1$) year could reduce dust emissions and forest fires in the following year (n) from enhanced soil and vegetation moisture. This could be a potential mechanism for the more significant effect of rainfall seen on TOMS Ai in the northeast (R1, a biomass burning region) and northwest (R6, desert region). However, a mechanism is not apparent for the effect of rainfall on TOMS Ai in the Indo-Gangetic plain (R3). We conclude that trends in anthropogenic emissions potentially affect aerosol load detected by TOMS.

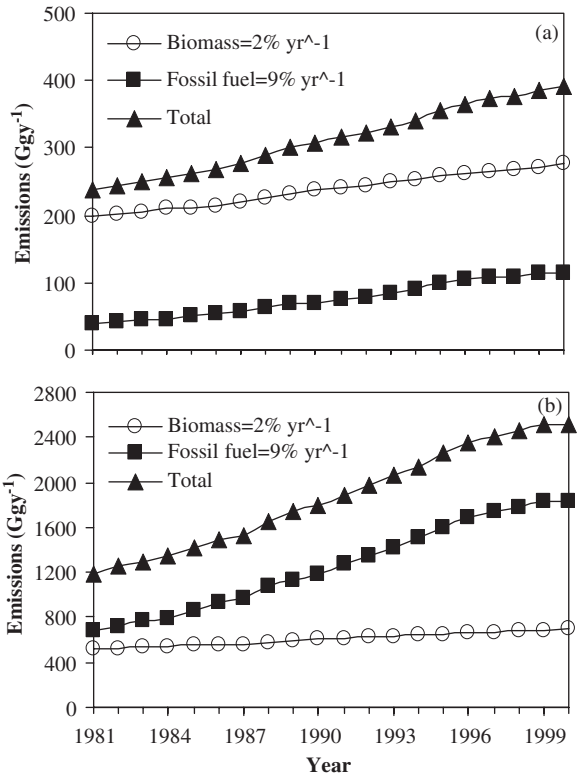

Fig. 7. Long-term trends in emissions of (a) BC and (b) IOM from fossil fuel and biomass combustion for India during 1981–2000.

4. Conclusions

This study presents an analysis of seasonal, spatial and interannual variability in absorbing aerosol loading over India, detected by TOMS during 1981–2000, in relation to estimated anthropogenic aerosol emission trends and regional meteorology, including rainfall and circulation

Table 1
Dependence of TOMS Ai on absorbing aerosol emissions, vertical velocity and annual rainfall (year $n-1$)

Regions	% Contribution to interannual variability in TOMS Ai				R^2	F^a	Significance-F^b
	Emissions	Vertical velocity	Rainfall	Unexplained			
R1	70	5	8	18	0.82	12	0.002
R2	56	0	5	38	0.62	4	0.044
R3	42	0	11	47	0.53	3	0.092
R4	73	1	4	21	0.79	10	0.005
R5	46	2	0	51	0.49	3	0.131
R6	37	1	7	55	0.45	2	0.163

[a] F is the ratio of the regression mean square to the residual mean square.

[b] F-significance is less than 0.05 then the hypothesis that there is no (linear) relationship can be rejected, and the multiple correlation coefficient can be called statistically significant.

patterns. Seasonal and spatial distributions in TOMS Ai were related to the anthropogenic and dust emission patterns in April–May, but modified by rainfall and regional atmospheric dispersion in January–March and rainfall in June–September except. The magnitude of TOMS Ai bore a relation to anthropogenic aerosol emission strength in all regions except those with a strong mineral dust loading. The seasonal cycle in TOMS Ai corresponded to the seasonal variability in dust or biomass burning emissions and to rainfall. Enhanced TOMS Ai in 1999 in northeast India, was potentially from forest burning emissions, deduced from its strong correlation with ATSR fire counts in this region. Trends in anthropogenic emissions during 1981–2000 potentially contribute to increases in the aerosol load detected by TOMS. This would need further investigation potentially through atmospheric simulations incorporating both trends in anthropogenic emissions and the interannual variability in natural sources of aerosols.

Acknowledgments

This work was supported by the Indo-French Center for the Promotion of Advanced Research (IFCPAR) under Project 1911-2. Additional investigator support (GH and CV) was provided by the Geosphere-Biosphere program of Indian Space Research Organization (ISRO-GBP). Chandra Venkataraman's visit to LOA in May 2004, was supported through the Indo-French Collaboration Program of the Embassy of France in India.

References

Anderson, T.L., Charlson, R.J., Schwartz, S.E., Knutti, R., Boucher, O., Rodhe, H., Heintzenberg, J., 2003. Climate forcing by aerosol—a hazy picture. Science 300, 1103–1104.

Arino, O., Simon, M., Piccolini, I., Rosaz, J.M., 2001. The ERS-2 ATSR-2 world fire atlas and the ERS-2 ATSR-2 world burnt surface atlas projects. Proceedings of the Eighth ISPRS Conference on Physical Measurement and Signatures in Remote Sensing, Aussois, 8–12 January.

Boucher, O., Haywood, J., 2001. On summing the components of radiative forcing of climate change. Climate Dynamics 18, 297–302.

Centre for Monitoring Indian Economy, 2001. Economic intelligence Service: Energy, New Delhi, India.

Chanda, T.K., Dubey, A.C., Sati, K., Robertson, C., 2001. Fertilizer Statistics. Report, Fertilizer Association of India, New Delhi, 434pp.

Chiapello, I., Prospero, J.M., Herman, R., Hsu, N.C., 1999. Detection of mineral dust over the North Atlantic Ocean and Africa with the Nimbus 7 TOMS. Journal of Geophysical Research 104, 9277–9291.

Di Girolamo, L., Bond, T.C., Bramer, D., Diner, D.J., Fettinger, F., Kahn, R.A., Martonchik, J.V., Ramana, J.V., Ramanathan, V., Rasch, P.J., 2004. Analysis of Multi-angle Imaging SpectroRadiometer (MISR) aerosol optical depths over greater India during winter 2001–2004. Geophysical Research Letters 31, L23115, doi:10.1029/2004GL021273.

Duncan, B.N., Martin, R.V., Staudt, A.C., Yevich, R., Logan, J.A., 2003. Interannual and seasonal variability of biomass burning emissions constrained by satellite observations. Journal of Geophysical Research 108 (D2), 4100.

Gabriel, R., Mayol-Bracero, O.L., Andreae, M.O., 2002. Chemical characterization of submicron aerosol particles collected over the Indian Ocean. Journal of Geophysical Research 107 (D19), 8005.

Gadgil, S., Srinivasan, J., Nanjundiah, R.S., Kumar, K.K., Munot, A.A., Kumar, K.R., 2002. On forecasting the Indian summer monsoon: the intriguing season of 2002. Current Science 83 (4), 394–403.

Generoso, S., Bréon, F.-M., Balkanski, Y., Boucher, O., Schulz, M., 2003. Improving the seasonal cycle and interannual variations of biomass burning aerosol sources. Atmospheric Chemisty Physics 3, 1211–1222.

Habib, G., Venkataraman, C., Shrivastava, M., Banerjee, R., Stehr, J., Dickerson, R., 2004. New methodology for estimating biofuel consumption for cooking: atmospheric emissions of black carbon and sulfur dioxide from India. Global Biogeochemical Cycles 18, GB3007.

Herman, J.R., Bhartia, P.K., Torres, O., Hsu, C., Seftor, C., Celarier, E., 1997. Global distribution of UV-absorbing aerosols from Nimbus 7/TOMS data. Journal of Geophysical Research 102 (D14), 16,911–16,922.

Hsu, N.C., Herman, J.R., Bhartia, P.K., Seftor, C.J., Torres, O., Thompson, A.M., Gleason, J.F., Eck, T.F., Holben, B.N., 1996. Detection of biomass burning smoke from TOMS measurements. Geophysical Research Letters 23, 745–748.

Hsu, N.C., Herman, J.R., Torres, O., Holben, B.N., Tanre, D., Eck, T.F., Smirnov, A., Chatenet, B., Lavenu, F., 1999. Comparison of the TOMS aerosol index with sun photometer aerosol optical thickness: results and applications. Journal of Geophysical Research 104 (D6), 6269–6279.

Husar, R.B., Prospero, J.M., Stowe, L.L., 1997. Characterization of tropospheric aerosols over the oceans with the NOAA advanced very high resolution radiometer optical thickness operational product. Journal of Geophysical Research 102, 16,889–16,910.

Li, F., Ramanathan, V., 2002. Winter to summer monsoon variation of aerosol optical depth over the tropical Indian Ocean. Journal of Geophysical Research 107 (D16), 4284.

Mayol-Bracero, O.L., Gabriel, R., Andreae, M.O., Kirchstetter, T.W., Novakov, T., Ogren, J., Sheridan, P., Streets, D.G., 2002. Carbonaceous aerosols over the Indian Ocean during the Indian Ocean Experiment (INDOEX): chemical characterization, optical properties and probable sources. Journal of Geophysical Research 107 (D19), 8030.

Moorthy, K.K., Nair, P.R., Prasad, B.S.N., Muralikrishnan, N., Gayathri, H.B., Narasimha Moorthy, B., Niranjan, K., Ramesh Babu, V., Satyanarayana, G.V., Agashe, V.V., Aher, G.R., Singh, R., Srivastava, B.N., 1993. Results from the WR Network of IMAP. Indian Journal of Radio and Space Physics 22, 243–258.

Moorthy, K.K., Saha, A., Prasad, B.S.N., Niranjan, K., Jhurry, D., Pillai, P.S., 2001. Aerosol optical depths over peninsular India and adjoining ocean during the INDOEX campaigns: spatial, temporal, and spectral characteristics. Journal of Geophysical Research 106, 28,539–28,554.

Novakov, T., Andreae, M.O., Gabriel, R., Kirchstetter, T.W., Mayol-Bracero, O.L., Ramanathan, V., 2000. Origin of carbonaceous aerosols over the tropical Indian Ocean: Biomass burning or fossil fuels. Geophysical Research Letters 27, 4061–4064.

Ramachandran, S., 2004. Spectral aerosol optical characteristics during the Northeast monsoon over the Arabian Sea and the tropical Indian Ocean: 1. Aerosol optical depths and their variabilities. Journal of Geophysical Research 109, D19207.

Ramachandran, S., Jayaraman, A., 2003. Ballon-borne study of the upper tropospheric and stratospheric aerosols over a tropical station in India. Tellus 55B, 820–836.

Ramanathan, V., Crutzen, P.J., Lelieveld, J., Mitra, A.P., Althausen, D., Anderson, J., Andreae, M.O., Cantrell, W., Cass, G.R., Chung, C.E., Clarke, A.D., Coakley, J.A., Collins, W.D., Conant, W.C., Dulac, F., Heintzenberg, J., Heymsfield, A.J., Holben, B., Howell, S., Hudson, J., Jayaraman, A., Kiehl, J.T., Krishnamurti, T.N., Lubin, D., McFarquhar, G., Novakov, T., Ogren, J.A., Podgorny, I.A., Prather, K., Priestley, K., Prospero, J.M., Quinn, P.K., Rajeev, K., Rasch, P., Rupert, S., Sadourny, R., Satheesh, S.K., Shaw, G.E., Sheridan, P., Valero, F.P.J., 2001. Indian Ocean Experiment: an integrated analysis of the climate forcing and effects of the great Indo-Asian haze. Journal of Geophysical Research 106, 28,371–28,398.

Reddy, M.S., Venkataraman, C., 2002a. A $0.25^\circ \times 0.25^\circ$ inventory of aerosol and sulfur dioxide emissions from India: I-fossil fuel combustion. Atmospheric Environment 36, 677–697.

Reddy, M.S., Venkataraman, C., 2002b. A $0.25^\circ \times 0.25^\circ$ inventory of aerosol and sulfur dioxide emissions from India: II—Biomass combustion. Atmospheric Environment 36, 699–712.

Reddy, M.S., Boucher, O., 2004. A study of global cycle of carbonaceous aerosols in the LMDZT general circulation model. Journal of Geophysical Research 109, D14202.

Reddy, M.S., Boucher, O., Venkataraman, C., 2002. Seasonal carbonaceous aerosol emissions from open biomass burning in India. Bulletin IASTA 14, 239–243.

Reddy, M.S., Boucher, O., Venkataraman, C., Verma, S., Léon, J.-F., Bellouin, N., Pham, M., 2004. General circulation model estimates of aerosol transport and radiative forcing during the Indian Ocean Experiment. Journal of Geophysical Research 109, D16205.

Satheesh, S.K., Srinivasan, J., 2002. Enhanced aerosol loading over Arabian Sea during the pre-monsoon season: natural or anthropogenic? Geophysical Research Letters 29, 1874.

Shrivastava, M., 2003. Trace gas emissions from biomass burning in India. M. Tech. Thesis, Indian Institute of Technology Bombay, Mumbai, India, 50pp.

Tegen, I., Fung, I., 1995. Contribution to the atmospheric mineral aerosol load from land surface modification. Journal of Geophysical Research 100, 18707–18726.

Torres, O., Bhartia, P.K., Herman, J.R., Ahmad, Z., Gleason, J., 1998. Derivation of aerosol properties from satellite measurements of backscattered ultraviolet radiation: theoretical basis. Journal of Geophysical Research 103, 17099–17100.

Venkataraman, C., Habib, G., Eiguren-Fernandez, A., Miguel, A.H., Friedlander, S.K., 2005. Residential biofuels in South Asia: carbonaceous aerosol emissions and climate impacts. Science 307, 1454–1456.